Accepted Manuscript

Application of spectroscopic methods (FT-IR, Raman, ECD and NMR) in studies of identification and optical purity of radezolid

Katarzyna Michalska, Ewa Gruba, Mikołaj Mizera, Kornelia Lewandowska, Elżbieta Bednarek, Wojciech Bocian, Judyta Cielecka-Piontek

PII:	S1386-1425(17)30306-2
DOI:	doi: 10.1016/j.saa.2017.04.038
Reference:	SAA 15091
To appear in:	*Spectrochimica Acta Part A: Molecular and Biomolecular Spectroscopy*
Received date:	4 November 2016
Revised date:	13 April 2017
Accepted date:	18 April 2017

Please cite this article as: Katarzyna Michalska, Ewa Gruba, Mikołaj Mizera, Kornelia Lewandowska, Elżbieta Bednarek, Wojciech Bocian, Judyta Cielecka-Piontek , Application of spectroscopic methods (FT-IR, Raman, ECD and NMR) in studies of identification and optical purity of radezolid. The address for the corresponding author was captured as affiliation for all authors. Please check if appropriate. Saa(2017), doi: 10.1016/j.saa.2017.04.038

Application of spectroscopic methods (FT-IR, Raman, ECD and NMR) in studies of identification and optical purity of radezolid

Katarzyna Michalska[1], Ewa Gruba[1], Mikołaj Mizera[2], Kornelia Lewandowska[3], Elżbieta Bednarek[4], Wojciech Bocian[4], Judyta Cielecka-Piontek[2]

[1] Department of Antibiotics and Microbiology, National Medicines Institute, Chełmska 30/34, 00-725 Warsaw, Poland

[2] Department of Pharmaceutical Chemistry, Faculty of Pharmacy, Poznan University of Medical Sciences, Grunwaldzka 6, 60-780 Poznan, Poland

[3] Department of Molecular Crystals, Institute of Molecular Physics of the Polish Academy of Sciences, Poznan, Poland

[4] Nuclear Magnetic Resonance Laboratory, National Medicines Institute, Chełmska 30/34, 00-725 Warsaw, Poland

Correspondence: Judyta Cielecka-Piontek
Department of Pharmaceutical Chemistry, Faculty of Pharmacy, Poznan University of Medical Sciences, Grunwaldzka 6, 60-780 Poznan, Poland
Tel.: +48 8546649, fax + 48 61 864 66 52

e-mail: jpiontek@ump.edu.pl

Katarzyna Michalska
Department of Antibiotics and Microbiology, National Medicines Institute, Chełmska 30/34, 00-725 Warsaw, Poland
Tel.: +48 22 851 52 15; fax: +48 22 851 52 15

e-mail: k.michalska@nil.gov.pl

Abstract:

In the presented study, *N*-{[(5*S*)-3-(2-fluoro-4′-{[(1*H*-1,2,3-triazol-5-ylmethyl)amino]methyl}biphenyl-4-yl)-2-oxo-1,3-oxazolidin-5-yl]methyl}acetamide (radezolid) was synthesized and characterized using FT-IR, Raman, ECD and NMR. The aim of this work was to assess the possibility of applying classical spectral methods such as FT-IR, Raman, ECD and NMR spectroscopy for studies on the identification and optical purity of radezolid. The experimental interpretation of FT-IR and Raman spectra of radezolid was conducted in combination with theoretical studies. Density functional theory (DFT) with the B3LYP hybrid functional was used for obtaining radezolid spectra. Full identification was carried out by COSY, ^{1}H {^{13}C} HSQC and ^{1}H {^{13}C} HMBC experiments. The experimental NMR chemical shifts and spin-spin coupling constants were compared with theoretical calculations using the DFT method and B3LYP functional employing the 6-311++G(d,p) basis set and the solvent polarizable continuum model (PCM). The experimental ECD spectra of synthesized radezolid were compared with experimental spectra of the reference standard of radezolid. Theoretical calculations enabled us to conduct HOMO and LUMO analysis and molecular electrostatic potential maps were used to determine the active sites of microbiologically active form of radezolid enantiomer. The relationship between results of *ab initio* calculations and knowledge about chemical-biological properties of *S*-radezolid and other oxazolidinone derivatives are also discussed.

Introduction

Studies concerning new entities at the early stage of R&D, subsequent in-process controls and finally control of the finished product, broadly defined as quality control, are often based on application of spectroscopic methods. UV and FT-IR, according to pharmacopeia guidelines, are the most frequently used for identification of selected drugs [1]. In the case of innovative drugs for which the effects of interactions with solvents have not been yet investigated, it is important to start studying them by characterization in the solid state. Hence spectroscopic methods are recommended for identification of novel drugs. FT-IR, Raman and NMR spectroscopy are simple and reproducible techniques for the analysis of drug racemates at different stages of development. The chiral analysis of drugs has also been extended by the connection of successive spectroscopic techniques with electronic circular dichroism (ECD) [2–5]. The possibility of studying enantiomers without using chiral selectors and organic solvents may be considered as a promising solution for quality control, especially in the field of optical drug isomerism. However, it should be stressed out, that the above-mentioned

spectroscopic techniques do not permit selective determination of the principal analyte in the presence of its impurities. This is only possible when suitable chemometric solutions are applied, allowing for the assessment of the type and concentration of a particular impurity based on predefined descriptors differentiating the API sample from its impurities.

The oxazolidinones are a novel class of synthetic antimicrobial agents, unrelated to any other class, showing a comprehensive spectrum of activity against the major and nosocomial Gram-positive pathogens, including methicillin-resistant *Staphylococcus aureus* (MRSA), enterococci and pneumococci [6]. The first oxazolidinone introduced into treatment was linezolid in 2000; the next agent – tedizolid – was approved in 2014. Radezolid (RX-1741) (Fig. 1) is a novel biaryloxazolidinone antibacterial agent which is in clinical development; two phase-2 clinical trials have been completed, the first in uncomplicated skin and skin-structure infections (uSSSI) and the second in community-acquired pneumonia (CAP) [7–9]. Radezolid emerged from the Rχ-01 discovery programme at Rib-X Pharmaceuticals, Inc., and revealed excellent antibacterial activity against linezolid-susceptible staphylococci, enterococci and pneumococci as well as against linezolid-resistant isolates, especially enterococci and pneumococci. Unlike linezolid, radezolid also showed proper antibacterial activity against the causative agents of CAP, such as *Haemophilus influenzae* and *Moraxella catarrhalis* [6].

In the oxazolidinone derivatives group, HPLC has been most frequently used for analysing linezolid and tedizolid in different matrices [10–12]. Capillary electrophoresis has also played a significant role in the analysis of linezolid and tedizolid [13–15]. Previously published studies confirmed the applicability of FT-IR and Raman spectra for identification of oxazolidinone derivatives and assessment of their chiral purity based on the analysis of ECD spectra [16–18]. Theoretical analysis of linezolid and tedizolid supported by density functional theory (DFT) calculations with 6-31G(d,p), 6-311G(d,p) and M06-2X/6-31G(d,p) basis sets allowed identification of the differences in molecular electrostatic potential (MEP) maps, which may be connected with their varied antimicrobial activity, and regions that indicate differing localization of electrons, which are connected to the chemical reactivity. Regarding spectroscopic bands important for identification of radezolid, such domains as triazole, biphenyl (including phenyl and 2-fluorophenyl moieties) and oxazolidinone rings as well as a methylacetamide substituent can be distinguished.

The aim of this study was identification of radezolid by application of FT-IR, Raman and NMR spectra, while ECD spectra were used for studies of the optical purity of radezolid. During the identification of the appropriate bands or chemical shifts and evaluation of their

intensity, FT-IR, Raman and NMR spectra analysis was supported by quantum chemical calculations using a Becke, 3-parameter, Lee-Yang-Parr (B3LYP) hybrid functional with a 6-31G(d,p) or 6-311++G(d,p) standard basis set. Based on the performed identification, a comparative analysis of radezolid enantiomers was executed, in regards to further evaluation of chiral purity. Additional characteristics were obtained to those previously achieved from spectra of radezolid by performing electronic properties tests such as HOMO-LUMO orbitals and MEPs for both (*R*)- and (*S*)- radezolid enantiomers.

Experimental methods

Substance for studies

Radezolid was synthesized as described in the supplementary information with slight improvements to the literature methods [19–21]. During experiments, as a reference material for comparison and of purity studies, single isomer (*S*)-radezolid from ApexBio Technology LLC (Houston, TX, USA) with 98% purity was used.

Spectroscopic methods

The vibrational infrared spectra of radezolid were recorded between 4000 and 100 cm^{-1} in powder, at room temperature, with a Bruker Equinox 55 FT-IR spectrometer equipped with a Bruker Hyperion 1000 microscope. Raman scattering spectra were obtained with a LabRAM HR800 spectrometer (HORIBA Jobin Yvon) with laser excitation λ_{exc} = 1064 nm (He-Ne laser). In each case the power of the laser beam focused on the sample was less than 1 mW to avoid damage of the sample. (*S*)-radezolid was established using a Jasco J-715 circular dichroism spectrometer. The ECD spectra of synthesized (*S*)-radezolid and its reference standard were recorded in water with the concentrations of 2.3 x 10^{-4} mol/L and 1.8 x 10^{-4} mol/L, respectively. The range of the ECD spectra was within 180–450 nm, with cell length 0.1 cm, scanning speed 100 nm/min, while the detector response was obtained every 0.5 s. All measurements were conducted at room temperature. The ^{1}H and ^{13}C NMR spectra of radezolid were recorded in D_2O (1.9 mg/mL) and DMSO-d_6 (8.0 mg/mL) solutions at 303 K using a Varian VN-MRS 500 spectrometer operated at 499.8 and 125.7 MHz for ^{1}H and ^{13}C, respectively. The full assignment of proton and carbon signals was accomplished using COSY, ^{1}H {^{13}C} HSQC and ^{1}H {^{13}C} HMBC experiments.

$^{1}H\{^{13}C\}$HSQCAD: an acquisition time of 0.15 s, relaxation delay of 1.0 s and spectral windows of 6000 Hz in F2 and 22600 Hz in F1. 512 complex data points were collected in the indirectly detected dimension (^{13}C) with 4 scans and 2048 points per increment. The data

were linearly predicted to 1K and zero filled to 4K complex data points in F1 and processed using the cosine window function in both dimensions prior to Fourier transformation. The proton and carbon π/2 pulse lengths were 6.75 and 14.8 μs, respectively.

^{1}H{^{13}C}-gHMBCAD: sweep width of 6000 Hz in F2 and 25150 Hz in F1, with an acquisition time of 0.17 s, relaxation delay of 1.0 s and ^{n}J(C,H) = 8 Hz. Overall, 512 complex data points were collected in the indirectly detected dimension (^{13}C) with 32 scans and 2048 points per increment. The data were linearly predicted to 1K and zero filled to 4K complex data points in F1 and processed using sine-bell square multiplication in F2 and Gaussian window function in F1 dimensions prior to Fourier transformation.

Computation details

The harmonic vibrational frequencies for spectroscopic analysis (for FT-IR and Raman spectra) were carried out with DFT using a B3LYP hybrid functional with a 6-31G(d,p) standard basis set and its variations with diffuse basis functions [22]. Obtained frequencies for FT-IR and Raman spectra were scaled by a factor of 0.961. Theoretical computation of optimal geometry, frontier molecular orbitals (FMOs) and MEP maps were calculated at the same level of theory for optimized structures. The NMR magnetic shielding and spin-spin coupling constants were calculated using the gauge-independent atomic orbital (GIAO) method [23] under DFT. The B3LYP functional employing the standard 6-311++G(d,p) basis set was used. The polarizable continuum model (PCM) using the standard integral equation formalism variant (IEFPCM) was used to mimic the influence of water as a solvent [24]. The GIAO calculations were preceded by precise searching for the lowest energy conformers conducted at the same level of theory. The NMR chemical shifts were calculated by a linear least squares method of fitting averaged values of NMR shieldings for the two lowest energy radezolid conformers (differing by mutual twisting of the fluorophenyl ring). All calculations were performed using Gaussian 09 software and visualized using GaussView [22].

Results and discussion

Identification of radezolid based on FT-IR and Raman spectra

For analysis of FT-IR and Raman spectra for detailed identification of the vibrational modes of radezolid, the following domains were separated: triazole ring, biphenyl ring (including the phenyl and 2-fluorophenyl moieties), oxazolidinone ring and methylacetamide substituent. The identification of characteristic spectral regions for radezolid was supported by comparing with theoretical spectra obtained based on DFT with the B3LYP hybrid functional and 6-

31G(d,p) basis set (Figs. 2 and 3). The calculated vibrational frequencies were scaled in order to improve agreement with experimental values. It is relevant to discuss the vibrational spectra of radezolid in terms of characteristic spectral regions as described below. The most characteristic bands associated with vibrations of the bonds present in the radezolid are located between 2000 and 500 cm^{-1}. The bands assignment of a vibrational model for the above-mentioned domains in the molecule in the FT-IR and Raman region are summarized in Table 1. In FT-IR and Raman spectra of radezolid, we observed many C–H bonds, and many bands related to them. Heteroaromatic organic compounds (in the case of triazole and biphenyl rings) and their derivatives are structurally very close to benzene and commonly exhibit multiple weak bands in the region 3100–3000 cm^{-1} due to the presence of C–H stretching vibrations [25]. For radezolid, bands related to the stretching vibration of C–H bonds were observed above 2500 cm^{-1}. In our study the bands were not as well resolved, that could be a result of intermolecular interaction. Besides that, characteristic bands were also observed related to the vibrations of the following bonds: C=O, C–O, C=C, C–C, C–N, N–N and C–F. Moreover, bands corresponding to the deformation of C–H bonds were also located in this range. In the FT-IR spectrum of radezolid there were better exposed and more intense bands than in the Raman spectrum. For example, in the FT-IR spectrum a quite strong band at 838 cm^{-1} is related to wagging vibration of the C–H bond in the triazole ring, while a strong band at 1136 cm^{-1} mainly corresponds to scissoring vibrations of the C–H bonds in the F-phenyl ring, but both of them have an additional component related to stretching vibration of the C–F bond. In contrast, the bands located on the slopes of wider bands at 1253 and 1486 cm^{-1} are related to twisting vibrations of the C–H bond in the methylacetamide substituent, scissoring vibrations of the C–H bonds in the oxazolidinone ring and rocking vibration of the C–H bonds in the phenyl and F-phenyl rings. In the Raman scattering spectrum bands corresponding to the vibration of C–H bonds were also observed; for example, at 553, 818, 900 and 1197 cm^{-1}, however they were very low in intensity. In contrast, very strong bands were observed in the Raman spectrum at 1617 and 1304 cm^{-1}, the first is associated with stretching vibration of the C=C bonds in the phenyl and F-phenyl rings, and the second is related to stretching vibration of the C–C bond between these rings and stretching vibration of this bond. The band at 1272 cm^{-1} is also related to stretching vibration of the C–C bond between the phenyl and F-phenyl rings. In the Raman spectrum the bands corresponding to stretching vibrations of the C–C bonds were also located at 1020 and 1217 cm^{-1}. The first band is related to vibration in the oxazolidinone ring, and the second is associated not only with stretching vibration of the C–C bond, but has additional components related to stretching

vibration of the C–N bond in the oxazolidinone ring, stretching vibration of the C–F bond and twisting vibration of the C–H bonds in the oxazolidinone ring, too. In the FT-IR spectrum we also observed stretching vibration of the C=C and C–C bonds; for example, the bands at 1293, 1530, 1561 and 1577 cm^{-1} correspond to stretching vibration of the C–C bonds in the phenyl and F-phenyl rings, vibrations between these rings and stretching vibration of the C=C and C–C bonds in the F-phenyl ring ring, respectively.

The characteristic peaks in the FT-IR spectrum at 1676 and 1754 cm^{-1} are related to stretching vibrations of the C=O bonds in the methylacetamide group and oxazolidinone ring, respectively. The other characteristic bands are those associated with stretching vibration of the C–N bonds. They are observed in the FT-IR spectrum at 1202, 1329 and 1379 cm^{-1}. The first band is mainly related to C–N vibrations in the oxazolidinone ring, but in this range we also observed additional components associated with rocking vibration of the C–H and N–H bonds in the triazole ring. The second band is related to stretching vibration of the C–N bonds between the triazole and oxazolidinone rings and in the oxazolidinone ring, and the last band corresponds to C–N vibration in both the oxazolidinone and triazole rings. In the lower frequencies bands related to bending vibration of the C–N–C bond in the [(methyl)amino]methyl group (for example 975 cm^{-1}) were also observed. Bands corresponding to N–H vibrations are also characteristic for radezolid. In our study bands related to stretching vibrations of those bonds were not easily visible; they were located above 3300 cm^{-1}, whereas at lower frequencies bands associated with the deformation vibration of these bonds were effortlessly observed. The bands of deformations in plane bending are assigned at 1417, 1442 and 1501 cm^{-1}, and are related to rocking vibrations in triazole ring and [(methyl)amino]methyl and methylacetamide substituents, respectively. It is worth pointing out, that vibrations belonging to C–X (F) bonds, which are formed between the ring and halogen atoms, are a mixture of vibrations. This is possible due to lowering of the molecules' symmetry and the presence of halogen atoms. C–F stretching vibrations appeared in the lower range of frequencies at 1400–1000 and 760–505 cm^{-1} and C–F deformations occurred in the range of 700–500 and 300–140 cm^{-1}. The bands which are mainly related to stretching and bending vibrations of C–F were located at 1199 and 480 cm^{-1}, respectively. Those bands were very often seen as an additional components in other bands (Table 1).

The assignments made in this study are also supported by the literature [26]. Bands characteristic of the key domains in molecules were defined for both of the oxazolidinone derivatives studied (linezolid, tedizolid) and attention was paid to signals registered for

carbon–fluorine bonds [16–18]. The number of bands and their intensity were greater in the case of FT-IR spectra.

NMR spectra

The results of NMR experiments in D_2O and DMSO-d_6 solutions are summarized in Table 2. In addition to ^{1}H and ^{13}C NMR chemical shifts, the values of selected spin-spin coupling constants (homo- and heteronuclear) are included. The presented data allowed us to fully confirm the molecular structure of radezolid and provide its full spectral characteristics in solutions. Additionally, theoretical calculations were made of both NMR chemical shifts and spin-spin coupling constants. Calculations were carried out using DFT with the B3LYP hybrid functional and 6-311++G(d,p) basis set. Simulations took into account the effect of the solvent by performing a reaction field calculation using IEFPCM. As the calculations were performed for the liquid state, it turned out to be necessary to consider the conformational mobility of the radezolid molecule. Sufficiently accurate results were obtained by averaging the calculated NMR data obtained for the two lowest energy radezolid conformers. These conformers differ only by torsional orientation of the fluorophenyl ring. The results of calculations are also presented in Table 2. Generally, the calculated and experimental values of NMR chemical shifts were in very good agreement. Some difficulties were observed only during comparison of the nuclear spin-spin couplings, which is not surprising, due to the lack of sophistication in available calculation methods. In the Table 2. are included only heteronuclear proton–fluorine and carbon–fluorine coupling constants as they seem to be the most characteristic and were calculated accurately enough.

Studies of chiral purity based on ECD spectra

An ECD technique was chosen as a reference measurement method for studies of the chiral purity of a radezolid enantiomer (Fig. 4). Comparison of the ECD spectra of a synthesized (*S*)-radezolid to an (*S*)-isomer serving as a reference standard, both dissolved in distilled water, confirmed that the differences found in the shapes of spectra curves were not significant. Those experiments also proved the stereoselective synthesis of (*S*)-radezolid. Radezolid showed a positive Cotton band with its maximum at 270 nm and a negative band with the maximum at 215 nm. Those observations suggest that the synthesized enantiomer did not contain any significant level of impurities of the chromophore structure, which could possibly lead to a change in the position of the absorption maxima and the shape of the spectra.

Frontier molecular orbitals

The HOMO (highest occupied molecular orbital) energy characterizes the ability of donating electrons while the LUMO (lowest unoccupied molecular orbital) energy characterizes the ability of accepting electrons [27–29]. The possibility of donating and withdrawing electrons by the triazole ring and the methylacetamide substituent was not observed. The HOMO is localized vertically on the biphenyl system whereas the LUMO is localized horizontally (Fig. 5). For the chiral centre at position C5 of the oxazolidinone structure no significant differences were found in the localization of electrons for the analysed FMOs. For radezolid E_{HOMO} and E_{LUMO} were −6.097 eV and −1.188 eV, respectively. Since the chemical potential of radezolid is negative, the compound is chemically stable and not prone to spontaneous degradation [30].

Molecular electrostatic potentials

Variations in electrostatic potential are largely responsible for the drug binding to receptor binding sites and hydrogen bonding interactions [31,32]. The MEP maps and their contours for radezolid generated with optimized geometry of the title molecule using GaussView software are shown in Fig. 6. The red and blue colours refer to electron-rich and electron-poor regions while the green area suggests almost neutral potentials. As a consequence, it is possible to predict the binding sites for electrophilic or nucleophilic attack in the molecule. Analysis of the MEP maps showed that two positive regions (blue) localized in the triazole and oxazolidinone rings correspond to the nucleophilic reactivity of radezolid. In the structure of oxazolidinone the nucleophilic area also comprises the chiral centre at position C5. It should be stressed out that the carbonyl groups in the methylacetamide substituent and the oxazolidinone structure are the sole negative regions responsible for the electrophilic reactivity of radezolid. Similar results were obtained for tedizolid and linezolid [16–19]. The differences in the MEP maps were observed at the 1,3-oxazolidin-2-one structure, which contains an asymmetric carbon atom, and is linked to the antibacterial activity of oxazolidinone derivatives [6].

Conclusions

The study involved experimental and theoretical spectroscopic analysis of (*S*)-radezolid – a novel oxazolidinone antibacterial agent – using FT-IR, Raman, NMR and ECD techniques with the support of the DFT theory. Theoretical analysis allowed to determination of charge transfer within the molecule and the calculated HOMO and LUMO energies demonstrated

that the molecule. was chemically stable. A plot of the MEPs showed the location of nucleophilic and electrophilic reactivity sites. The application of FT-IR, Raman and NMR techniques can be recommended for identification of radezolid both in solid and in solution states whereas the use of ECD spectra was found to be suitable for evaluating the chiral purity of microbiologically active (*S*)-radezolid. However, each of the proposed spectroscopic methods should be considered as a preliminary step valuable for principal identification of the analyte but not allowing for its assay in the presence of related sustances.

Acknowledgments

This study was supported by a SONATA grant from the National Science Centre, Poland (UMO-2013/11/D/NZ7/01230).

This research was supported in part by PL-Grid Infrastructure.

References

[1] European Pharmacopoeia 8th Edition - EDQM (2016).

[2] C. Bertucci, M. Pistolozzi, A. De Simone, Anal Bioanal Chem. 398 (2010) 155–166.

[3] Y. He, B. Wang, R.K. Dukor, L.A. Nafie, Appl. Spectrosc. 65 (2011) 699–723.

[4] A. Ganesau, M. Brunger, F. Wang, Eur. Phys. J. 67 (2013) 229–232.

[5] N. Rahman, S. Khan, Circular dichroism spectroscopy: Spectrochim. Acta A Mol. Biomol.Spectrosc.160 (2016) 26–33.

[6] K. Michalska, I. Karpiuk. M. Król, S. Tyski, Biorganic & Med. Chem. 21 (2013) 577–591.

[7] E. Skripkin, T.S. McConnell, J. DeVito, L. Lawrence, J.A. Ippolito, E.M. Duffy, J. Sutcliffe, F. Franceschi, Antimicrob. Agents Chemother. 52 (2008) 3550-7.

[8] G. Zhanel, R. Love, H. Adam, A. Golden, S. Zelenitsky, F. Schweizer, B. Gorityala, P. Lagace-Wiens, E. Rubinstein, A. Walkty, A. Gin, M. Gilmour, D. J. Hoban, J. Lynch 3rd, J.A. Karlowsky, Drugs, 75 (2015) 253–270.

[9] S. Lemaire, P. M. Tulkens, F. Van Bambeke, Antimicrob. Agents Chemother. 54 (2010) 2540-2548.

[10] A. Bielejewska, K. Duszczyk, J. Żukowska, Acta Chromatographic, 15 (2005) 183–191.

[11] L. Baietto, A. D'Avolio, A. Ariaudo, S. Corcione, M. Siemiele, J. Cusato, R. Urbino, G. Di Perri, V.M. Ranieri, F. G. De Rosa, J Chromatogr. B, 936 (2013) 42-47.

[12] H. Yu, C. Pan, Q. Xie, Y. Zheng, Y. Hu, Y. Lin, J. Chromatogr. B, 1011 (2016) 94-98.

[13] K. Michalska, G. Pajchel, S. Tyski, J. Pharm. Biomed. Anal. 48 (2008) 321–330.

[14] K. Michalska, G. Pajchel, S. Tyski, J. Chromatogr. A 1180 (2008) 179-186.

[15] K. Michalska, E. Gruba, J. Cielecka-Piontek, E. Bednarek, J. Pharm. Biomed. Anal., 120 (2016) 402-412.

[16] K. Rajalakshmi, S. Gunasekaran, S. Kumaresan, Indian J. Phys. 89 (2015) 525–538.

[17] R.J. Xavier, A. Prabaharan, Spectrochim. Acta A Mol. Biomol. Spectrosc. 136 (2015) 1530–1542.

[18] K. Michalska, M. Mizera, K. Lewandowska, J. Cielecka-Piontek, J. Mol. Struc. 1115 (2016) 136-143.

[19] W.B Im, S.H. Choi, J.-Y. Park, S.H. Choi, J. Finn, S.-H. Yoon, Eur. J. Med. Chem. 46 (2011) 1027-1039.

[20] M.R. Barbachyn, Patent Application Pub. No.: WO 94/13649; Pub. Date: Jun. 23, 1994; Tropone-substituted phenyloxazolidinone antibacterial agents.

[21] M.B. Gravestock, H.K. Huynh, N.J. Hales, Patent Application Pub. No.: US 2006/0058314 A1; Pub. Date: Mar. 16, 2006; Oxazolidinone derivatives and their use as antibacterial agents.

[22] Gaussian Gausssian 09, Revision A.01, M. J. Frisch, G. W. Trucks, H. B. Schlegel, G. E. Scuseria, M. A. Robb, J. R. Cheeseman, G. Scalmani, V. Barone, B. Mennucci, G. A. Petersson, H. Nakatsuji, M. Caricato, X. Li, H. P. Hratchian, A. F. Izmaylov, J. Bloino, G. Zheng, J. L. Sonnenberg, M. Hada, M. Ehara, K. Toyota, R. Fukuda, J. Hasegawa, M. Ishida, T. Nakajima, Y. Honda, O. Kitao, H. Nakai, T. Vreven, J. A. Montgomery, Jr., J. E. Peralta, F. Ogliaro, M. Bearpark, J. J. Heyd, E. Brothers, K. N. Kudin, V. N. Staroverov, R. Kobayashi, J. Normand, K. Raghavachari, A. Rendell, J. C. Burant, S. S. Iyengar, J. Tomasi, M. Cossi, N. Rega, J. M. Millam, M. Klene, J. E. Knox, J. B. Cross, V. Bakken, C. Adamo, J. Jaramillo, R. Gomperts, R. E. Stratmann, O. Yazyev, A. J. Austin, R. Cammi, C. Pomelli, J. W. Ochterski, R. L. Martin, K. Morokuma, V. G. Zakrzewski, G. A. Voth, P. Salvador, J. J. Dannenberg, S. Dapprich, A. D. Daniels, O. Farkas, J. B. Foresman, J. V. Ortiz, J. Cioslowski, and D. J. Fox, Gaussian, Inc., Wallingford CT, 2009.

[23] J. R. Cheeseman, G. W. Trucks, T. A. Keith, and M. J. Frisch, “A Comparison of Models for Calculating Nuclear Magnetic Resonance Shielding Tensors,” J. Chem. Phys., 104 (1996) 5497-509.

[24] G. Scalmani and M. J. Frisch, “Continuous surface charge polarizable continuum models of solvation. I. General formalism,” J. Chem. Phys., 132 (2010) 114110.

[25] M El-Nahass, M A Kamel, A F El-deeb, A A Atta and S Y Huthaily Spectrochim. Acta Part A 79 443 (2011).

[26] M. Prabhaharan, A.R. Prabakaran, S. Srinivasan, S. Gunasekaran, Spectrochim. Acta A Mol. Biomol. Spectrosc. 138 (2015) 711–722.

[27] N. Sinha, O. Prasad, V. Narayan, S.R. Shukla, J. Mol. Simul. 37 (2011) 153–163.

[28] D.F.V. Lewis, C. Loannides, D.V. Parke, Xenobiotica 24 (1994) 401–408.

[29] B. Kosar, C. Albayrak, Spectrochim. Acta A 78 (2011) 160–167.

[30] R. Ulahannan, C.Y. Panicker, H. T. Vargese, L.K. Srivastava, Spectrochim. Acta A 151 (2015) 184–197.

[31] E. Scrocco, J. Tomasi, Adv. Quantum Chem. 103 (1978) 115–193.

[32] F.J. Luque, J.M. Lopez, M. Orozco, Theor. Chem. Acc. 103 (2000) 343–345.

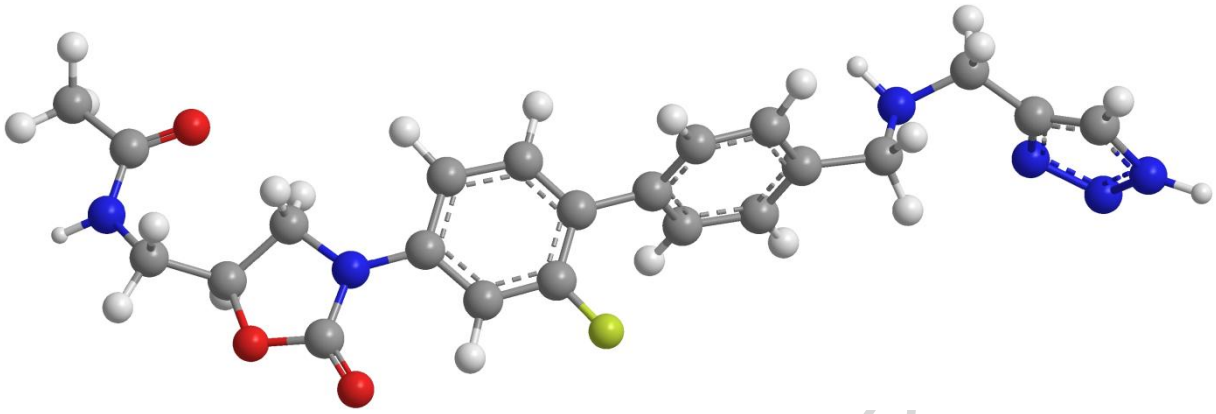

Fig. 1. Chemical structure of (S)-radezolid.

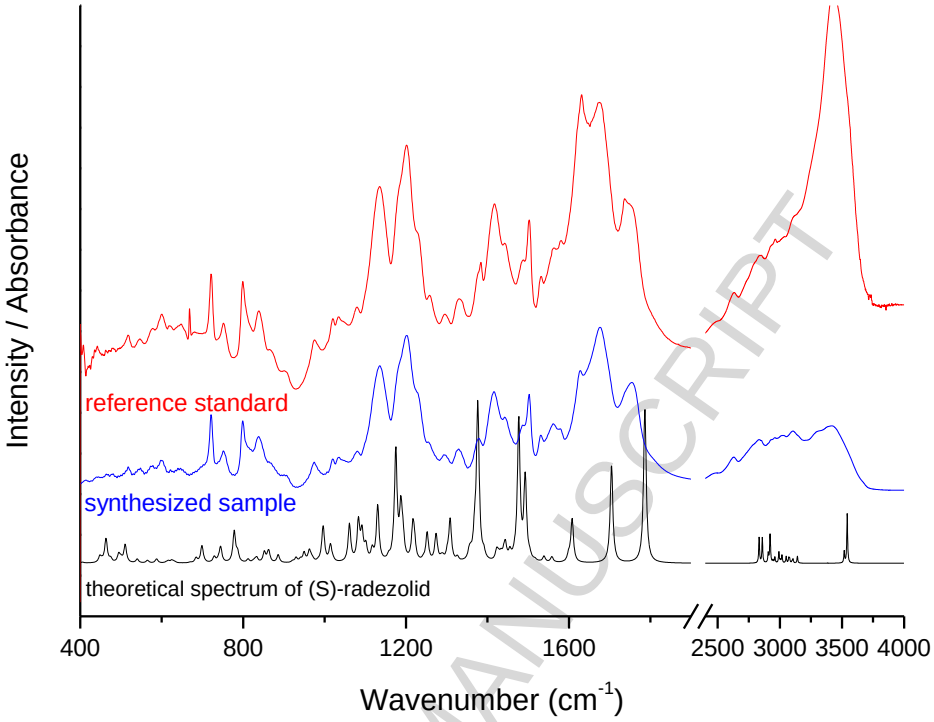

Fig. 2. The calculated (black), synthesized sample (blue), and reference standard (red) FT IR absorption spectra in room temperature of (S)-radezolid.

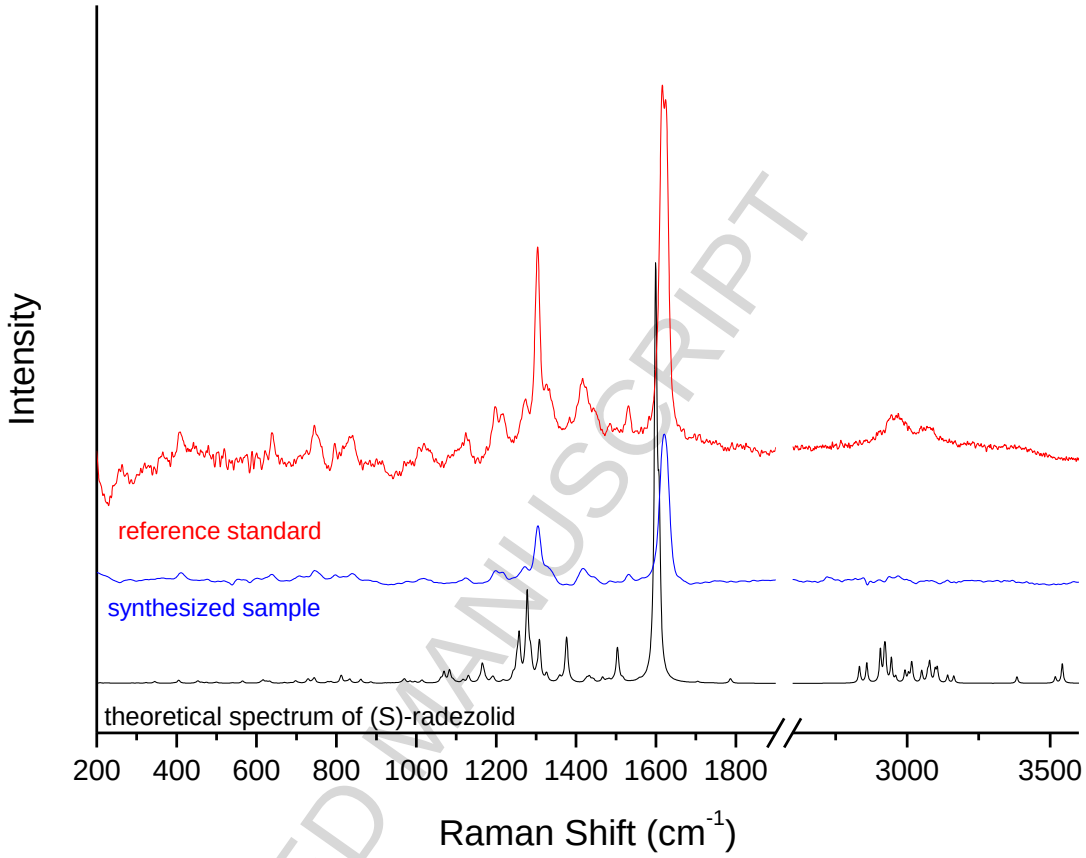

Fig. 3. The calculated (black), synthesized sample (blue) and reference standard (red) Raman scattering spectra in room temperature of (S)-radezolid.

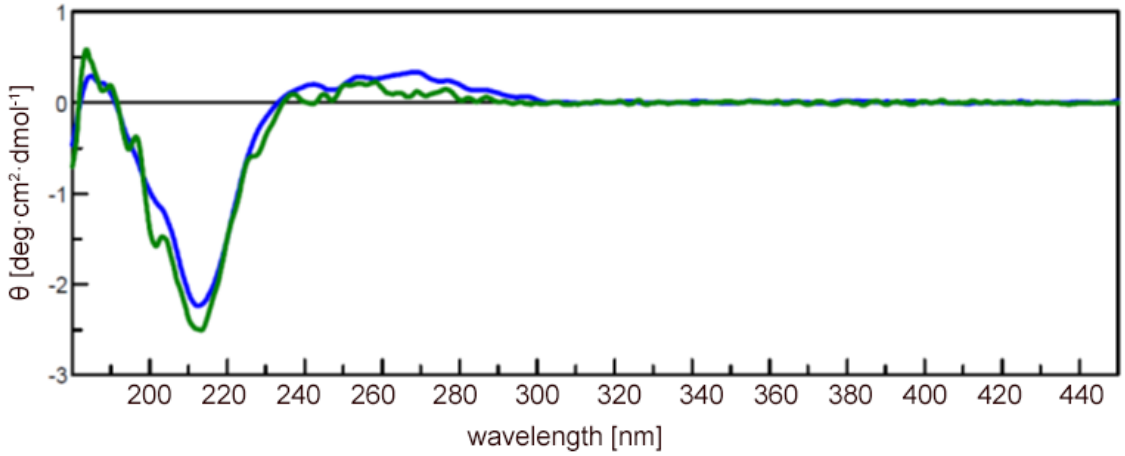

Fig. 4. Experimental of UV-CD spectra for synthetized (*S*)-radezolid (blue) and ApexBio reference standard of (*S*)-radezolid (green).

A.

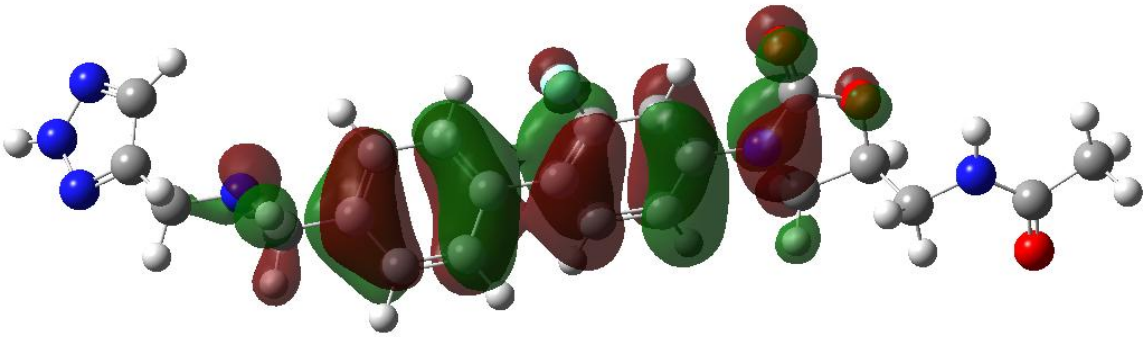

B

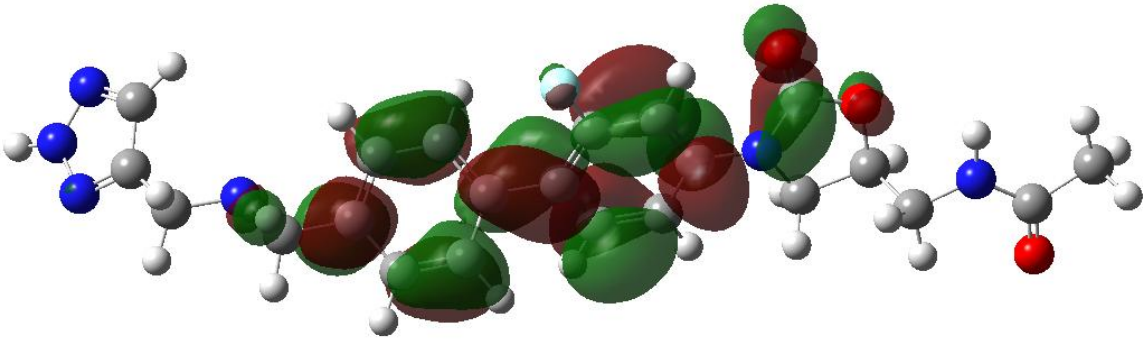

Fig. 5 The frontier molecular orbitals for (S)-radezolid: HOMO (A) and LUMO (B)

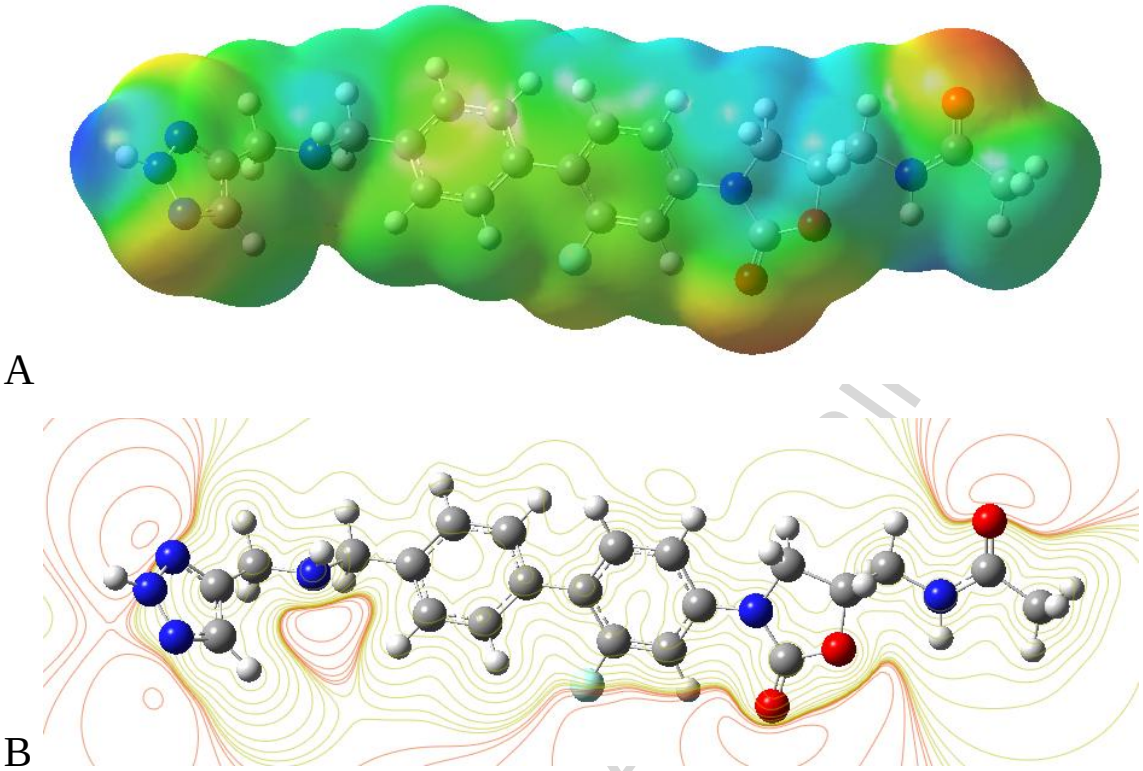

Fig. 6. Spatial (A) and contour (B) molecular electrostatic potential map (MEP) for (S)-radezolid.

Table 1. Comparison of the selected vibrations observed experimental and calculated (B3(LYP/6-31G(d,p) spectra of radezolid

$\nu_{exp.IR}$	$\nu_{exp.R}$	$\nu_{t.}$	Bands assignment
	410	405	def. all molecule
480		473	C-F *b*
515		509	N-H *w* in triazole ring
	553	564	C-H *w*
597	600	615	def 2-fluorophenyl ring
722	724	698	N-H *w* in triazole ring
	743	744	C-C-O *b* in oxazolidinone ring + C-C-N *b* in triazole ring and in (methyl)amino group
750		777	N-H *w* in triazole ring
	779	786	N-H *w* in (methyl)amino group + C-H *w* in 2-fluorophenyl ring
	797	811	Breathing phenyl ring + C-H *w* phenyl ring + N-H *w* in (methyl)amino group
	818	832	C-H *w* in phenyl ring
838		851	C-H *w* in triazole ring
	839	860	Breathing 2-fluorophenyl ring and oxazolidinone ring + C-N *s* in oxazolidinone ring + C-C *s* in o oxazolidinone ring + C-F *s* in 2-fluorophenyl + C-H *r* in oxazolidinone ring
	900	885	C-H *r* in oxazolidinone ring ring
975	976	969	C-N-C *b* in łącznik + C-H *t* łącznik + C-C *s* in triazole ring
	1005	984	Breathing phenyl and 2-fluorophenyl ring (C-C *s*)
1020	1020	1014	C-C *s* in oxazolidinone ring
	1109	1068	C-N-C *b* + C-H *t* in (methyl)amino group
	1121	1083	C-H *r* in 2-fluorophenyl ring + C-N *s* in oxazolidinone ring
1136		1130	C-H *sc* in 2-fluorophenyl ring + C-F *s* in 2-fluorophenyl ring
	1161	1156	C-H *r* in 2-fluorophenyl ring + C-F *s* in 2-fluorophenyl ring
	1197	1164	C-H *w* in phenyl ring
1199		1173	C-F *s* in 2-fluorophenyl ring + C-H *w* in oxazolidinone ring
1202		1186	C-N *s* in oxazolidinone ring + C-H *r* + N-H *r* in triazole ring
	1217	1192	C-C *s* between phenyl ring and (methyl)amino group + C-N *s* in oxazolidinone ring + C-F *s* in 2-fluorophenyl ring + C-H *t* in oxazolidinone ring
1225		1216	N-N *r* in methylacetamid group+ C-C *s* in methylacetamid group + C-H *r* 2-fluorophenyl ring + C-H *w* in methylacetamid group
1253		1251	C-H *t* in methylacetamid group
	1272	1257	C-C *s* between phenyl and 2-fluorophenyl ring
1293		1273	C-C *s* in phenyl and 2-fluorophenyl ring + C-H *w* in phenyl ring and (methyl)amino group
	1304	1277	C-C *s* between phenyl and 2-fluorophenyl ring + C-C *s* in phenyl and 2-fluorophenyl ring

1329	1326	1307	C-N *s* between 2-fluorophenyl and oxazolidinone ring + C-N *s* in triazole ring + C-H *r* in phenyl ring
1379	1423	1376	C-N *s* in oxazolidinone ring and triazole ring + C-H *w* in oxazolidinone ring
1417	1416	1433	N-H *r* in triazole ring + (methyl)amino group
1442		1443	N-H *r* in (methyl)amino group
1486		1476	C-H *sc* in oxazolidinone ring ring + C-H *r* in phenyl and 2-fluorophenyl ring
1501		1492	N-H *r* in methylacetamid group
1530	1530	1502	C-C between phenyl and 2-fluorophenyl ring + C-H *r* in phenyl and 2-fluorophenyl ring
1561		1538	C=C *s* + C-C *s* in phenyl and 2-fluorophenyl ring
1577		1557	C-C *s* in phenyl and 2-fluorophenyl ring
1629	1617	1598	C=C *s* in phenyl and 2-fluorophenyl ring
1629	1617	1607	C=C *s* in phenyl and 2-fluorophenyl ring
1676		1703	C=O *s* in methylacetamid group
1754		1786	C=O *s* in oxazolidinone ring

All positions in cm^{-1}; s-stretching, b-bending, r-rocking, w-wagging, sc-scissoring, oop-out of the plane.

Table 2. The experimental and calculated NMR data (δ -chemical shifts [ppm] of ^{1}H and ^{13}C atoms and *J* coupling constants[Hz}) of Radezolid

	synthesized (*R*)-radezolid –D2O		**APEX-BIO -(*S*)-radezolid –D2O**		**synthesized (*S*)-radezolid –DMSO**		**Calculated DFT PCM(H_2O)**	
	^{1}H	^{13}C	^{1}H	^{13}C	^{1}H	^{13}C	^{1}H	^{13}C (^{15}N)
2C=O	-	159.42	-	159.49	-	153.90	-	156.48
4CH_2	3.88 (dd, 1H, *J* = 6.0, 9.4 Hz) 4.25 (dd, 1H, *J* = 8.9, 9.4 Hz)	50.93	3.93 (dd, 1H, *J* = 6.0, 9.4 Hz) 4.28 (dd, 1H, *J* = 8.9, 9.4 Hz)	50.96	3.79 (dd, 1H, *J* = 6.4, 9.3 Hz) 4.17 (dd, 1H, *J* = 8.8, 9.3 Hz)	47.10	3.96 4.02	49.12
5CH	4.89 – 4.94 (m, 1H)	75.79	4.91 – 4.96 (m, 1H)	75.82	4.75 – 4.80 (m, 1H)	71.71	4.96	77.01
6CH_2	3.59 (dd, 1H, *J*= 5.4, 14.9 Hz) 3.63 (dd, 1H, *J* = 3.9, 14.9 Hz)	44.67	3.61 (dd, 1H, *J* = 5.4, 14.9 Hz) 3.65 (dd, 1H, *J* = 3.9, 14.9 Hz)	44.66	3.44 (dd, 2H, *J* = 5.5 Hz)	41.29	4.01	41.47
7NH	-	-	-	-	8.26 (t, 1H, *J* = 6 Hz, N**H**$COCH_3$)	-	5.83	-
8C=O	-	177.79	-	177.82	-	169.94	-	(173.01)
9CH_3	2.01 (s, 3H)	24.69	2.01 (s, 3H)	24.69	1.84 (s, 3H)	22.35	2.24	23.89
1'C	-	141.39	-	141.40	-	139.51 (J^{CF} = 11.1 Hz)	-	142.34 (J^{CF} = 9.3 Hz)
2'CH	7.48 (dd, 1H, *J* = 2.3, 12.9 Hz)	110.08 (J^{CF} =28.3 Hz)	7.50 (dd, 1H, *J* = 2.3, 12.9 Hz)	110.16 (J^{CF} = 28.3 Hz	7.63 (1H)	105.48 (J^{CF} = 28.6 Hz)	7.16 (J^{HF}=14.9 Hz)	106.12 (J^{CF} = 28.9 Hz)
3'CF	-	162.34	-	162.32 (J^{CF} = 243.7 Hz)	-	158.92 (J^{CF} = 244.9 Hz)	-	163.74 (J^{CF} =-316.2 Hz)
4'C	-	126.73	-	126.75	-	122.02 (J^{CF} = 13.5 Hz)	-	126.76 (J^{CF} = 10.9 Hz)
5'CH	7.57 (dd, 1H, *J* = 8.6, 8.6 Hz)	133.90	7.59 (dd, 1H, *J* = 8.6, 8.6 Hz)	133.93 (J= 4.7 Hz)	7.60 (1H)	130.78 (J^{CF} = 4.5 Hz)	7.59 (J^{HF}= 8.2 Hz)	133.45 (J^{CF} = 2.6 Hz)
6'CH	7.34 (dd, 1H, *J* = 2.3, 8.6 Hz)	118.04	7.36 (dd, 1H, *J* = 2.3, 8.6 Hz)	118.12 (J= 3.5 Hz)	7.44 (dd, 1H, *J* = 2.2, 8.6 Hz)	113.84 (J^{CF} = 3.2 Hz)	7.88 (J^{HF}=-1.1 Hz)	115.50 (J^{CF} = 4.3 Hz)
1"C	-	139.15		139.17	-	135.23 (J^{CF} = 1.8 Hz)	-	138.16 (J^{CF} =-2.0 Hz)
2"CH / 6"CH	7.68 (dd, 2H, *J* = 1.6, 8.3 Hz)	132.46	7.69 (dd, 2H, *J* = 1.6, 8.3 Hz)	132.48	7.62 (2H)	128.75 (J^{CF} = 3.1 Hz)	7.72	131.00 (J^{CF} =6.5, 0.0 Hz)
3"CH / 5"CH	7.57 (d, 2H, *J* = 8.3 Hz)	133.09	7.58 (d, 2H, *J* = 8.3 Hz)	133.09	7.66 (2H)	130.33	7.77	131.73

4''C	-	132.82	-	132.85	-	130.96	-	143.45
4'''CH	8.07 (br. s, 1H, triazole)	n.d.	8.07 (br. s, 1H, triazole)	n.d.	7.98 (br. s, 1H, triazole)	n.d.	7.72	132.84
5'''C	-	140.11	-	140.10	-	138.12	-	141.94
6''' CH_2	4.50 (br. s, 2H)	43.65	4.50 (br. s, 2H)	43.67	4.33 (br. s, 2H)	40.73	4.21	45.79
8''' CH_2	4.37 (br. s, 2H)	53.10	4.38 (br. s, 2H)	53.11	4.27 (br. s, 2H)	49.35	4.20	57.80
N^+H_2	-	-	-	-	9.51 (br. s, 2H, $ArCH_2N^+H_2$)	-	-	(156.48)

Graphical abstract

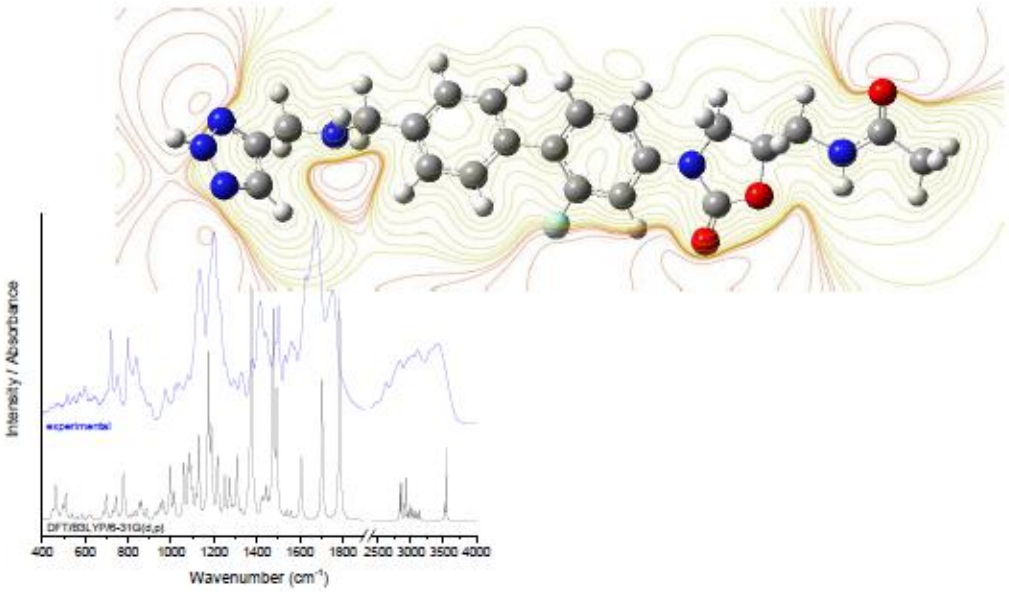

Highlights

- Raman, FT-IR, NMR and UV-CD spectra of radezolid were established
- Geometric structure of molecules, HOMO and LUMO orbitals and MEP were determined
- Benefits of applying FT-IR, Raman, NMR and UV-CD spectroscopy were signed